

Numerical and experimental study for process improvement of cross-wedge rolling of bearing steel balls

Jiapeng Wang¹, Baoyu Wang^{1,2*}, Chaoyang Sun¹, and Chuanbao Zhu³

¹School of Mechanical Engineering, University of Science and Technology Beijing, 100083 Beijing, China

²Engineering Research Center of Part Rolling, Ministry of Education, 100083 Beijing, China

³Shandong Zhongxing Auto Parts Ltd Company, Lixin Town, Laiwu City, 271126 Shandong Province, China

Abstract. The uniaxial compression experiments were conducted on GCr15 bearing steel to obtain the flow stress curves under hot deformation conditions. Based on the results of uniaxial compression experiments, finite element modeling was conducted on the cross wedge rolling (CWR) of GCr15 bearing steel balls, and numerical simulation was conducted using Simufact Forming 16.0. The results show that the distribution of effective strain of existing CWR steel balls is uneven, which may lead to uneven quality of steel balls. In addition, the three principal stresses at the center of the steel balls are all tensile stresses, and the effective stress at the center of the middle ball is relatively large, which can easily induce central defects. Moreover, different diameter billets were used for steel balls rolling experiments. It can be seen that when the die cavity is underfilled with billet, the rolled steel balls have no central defects. When the die cavity is fulfilled with billet, there is central piercing appearing at the middle ball, while the side balls have no obvious central defects. Finally, the paper proposes the method of even numbered ball rolling (ENBR) which starts from the middle connector to improve the CWR process of steel balls.

1 Introduction*

Bearing steel balls, as rolling elements in bearings, are used between bearing rings to carry loads and reduce friction, which are widely used in fields such as automobiles and aerospace [1]. The existing production methods mainly include hot forging, rolling, and cold heading. Among them, the rolling process has obvious technological advantages due to its high production efficiency and high material utilization rate [2].

At present, the ball rolling process mainly includes skew rolling and cross wedge rolling. Pater et al. [3] used a combination of numerical simulation and experiments to study the forming process of helical wedge rolling steel balls, proving that the helical wedge rolling process can be employed to form spherical parts and the production efficiency can be

* Corresponding author: bywang@ustb.edu.cn

improved through multi-wedge dies. Bulzak et al. [4] studied the skew rolling process of 100Cr6 bearing steel balls and analyzed the microstructure and surface roughness of the obtained steel balls. Cao et al. [5] conducted finite element simulation research on the cold skew rolling process of 7.4 mm diameter bearing steel balls. Pater et al. [6] proposed the use of cross wedge rolling process for producing steel balls from scrap rail heads and the feasibility was verified through corresponding experiments.

Cross wedge rolling process has been used in the production of shaft parts due to its stability, reliability, and high forming accuracy [7]. Currently, there is limited research on the use of cross wedge rolling technology for producing steel balls. Wang et al. [8] proposed a novel method for ball forming by cross wedge rolling and the corresponding finite element simulation and experimental research were conducted using 26 mm steel balls as an example. How to enrich more process possibilities and better apply cross wedge rolling technology to precision production of bearing steel balls has always been of utmost importance.

2 Materials and finite element modeling

2.1 Materials

The materials used is spheroidized annealed GCr15 bearing steel, and its main chemical composition is shown in Table 1. In order to obtain the true stress-strain curves of GCr15 bearing steel, the uniaxial compression experiments were conducted. The specimen size was $\phi 8 \times 12$ mm cylinder and the uniaxial compression experiments were conducted on Gleeble 1500D, as shown in Fig. 1a. The specimens undergoes four stages in sequence from Fig. 1b: rapid heating at 10 °C/s (A), holding for 3 mins (B), uniaxial compression (C), and water quenching (D). In addition, considering the characteristics of the CWR steel balls, the deformation temperature is 950/1000/1050/1100 °C and the deformation rate is 0.1/1/20 s⁻¹. The true stress-strain curves of GCr15 bearing steel under different deformation conditions are shown in Fig. 2.

Table 1. Main chemical composition of the GCr15 bearing steel

Element	C	Cr	Si	Mn	Mo	Fe
Wt %	0.99	1.40	0.36	0.30	0.095	balance

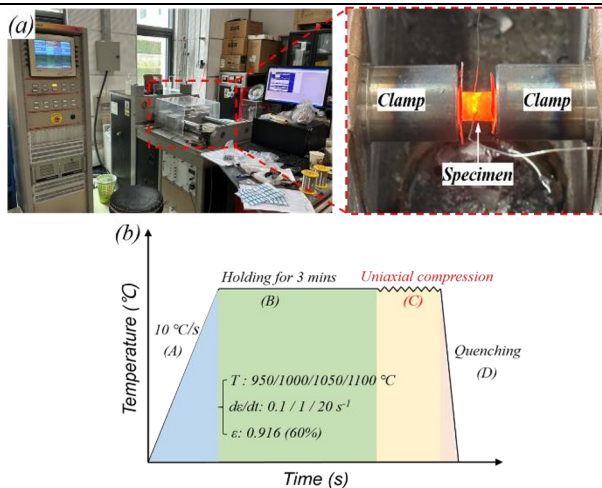


Fig. 1. a Diagram of uniaxial compression equipment and b schematic diagram of experimental process

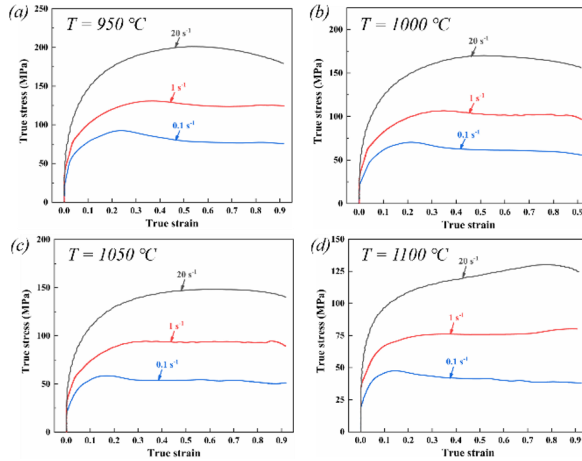


Fig. 2. Stress-strain curves of GCr15 bearing steel at different temperatures

2.2 Finite element modeling

Figure 3 shows the principle of CWR bearing steel balls and a schematic diagram of finite element modeling. The rolling process starts from the middle of the billet to form the middle ball, and then spreads to two sides to form the side balls in sequence. The finite element model, which includes two identical rollers and guide plates, and the billet, was numerically simulated using Simufact 16.0 software. The flow behavior of the billet material GCr15 bearing steel is based on the results obtained from the above experiments. Besides, the tools are regarded as rigid bodies for negligible elastic deformation and the contact surface between the billet and tools adopts a shear friction model [8]. It is worth noting that the forming angle of the roller are equal diameter circular arcs of R13. The detailed numerical simulation parameters are shown in Table 2.

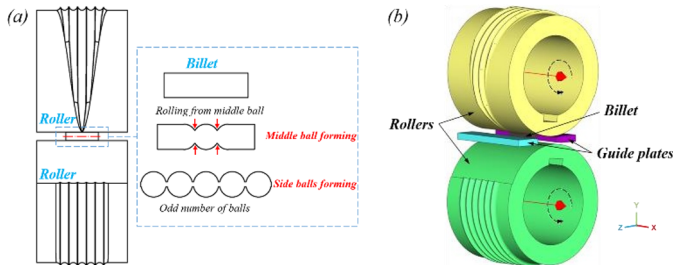


Fig. 3. **a** Principle of CWR bearing steel balls and **b** corresponding finite element modeling diagram

Table 2. Detailed numerical simulation parameters

Parameter	Value
Initial temperature of billet (°C)	1050
Temperature of tools and environment (°C)	20
Billet diameter/target ball diameter (mm)	25/26
Roller base circle diameter (mm)	374
Speed of roller (Rpm)	10
Friction factor: billet and rollers/guide plates	0.99/0.3
Heat transfer coefficient: billet and tools/environment (kW/m ² k)	10/0.3
Spreading angle of roller (°)	8
Forming angle of roller (mm)	R13

3 Results and Discussion

3.1 Numerical simulation results

Figure 4 shows the distribution of effective strain during the forming process of steel balls by CWR. From the figure, it can be seen that the forming process starts from the middle of the billet, and the middle of the billet is gradually formed into a middle ball by rotating and squeezing with the gradual rise of wedges of roller. Secondly, the wedges on both sides gradually extrude the billet to form two balls on both sides and propagate continuously until the forming process is completed. It is worth noting that the effective strain of the middle ball which is simultaneously subjected to the extrusion of two wedges is significantly higher than that of the side balls which is subjected to the extrusion of only one wedge, which cause differences in the forming characteristics between the middle ball and the side balls.

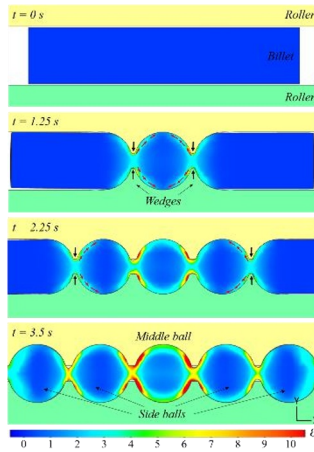


Fig. 4. Effective strain distribution of CWR steel balls

Moreover, the difference in stress distribution between the middle ball and side balls is shown in Fig. 5. It can be seen that the principal stresses on the surface of the steel balls are all compressive stresses, while the principal stresses at the center of the balls are all tensile stresses. In order to compare the stress levels at the center of steel balls in different positions, the middle ball, side ball 1 and side ball 2 (shown in Fig. 5a) were selected for comparison as shown in Fig. 5b. It can be seen that the maximum principal stress and effective stress of the middle ball are significantly greater than those of the two side balls, indicating that the middle ball is most likely to cause loose defects in the center.

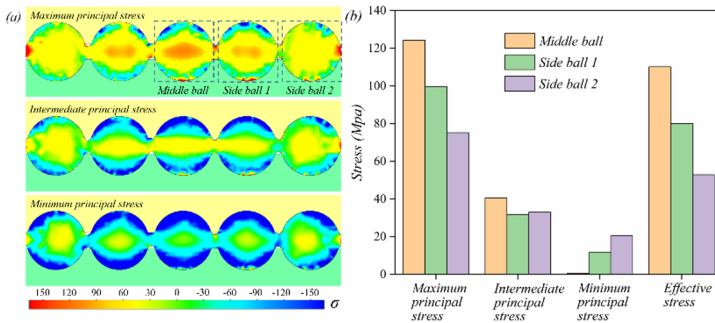


Fig. 5. a Principal stress distribution of CWR steel balls and **b** the comparison of stress at the center of different steel balls

3.2 Experimental results

The experimental parameters of CWR bearing steel balls are the same as the finite element model parameters. The GCr15 bearing steel rod with a diameter of 25 mm was heated to 1050 °C for 10 mins and then quickly transferred to the rolling mill for CWR experiments. The rolling mill, rollers and bearing steel balls obtained in the experiment are shown in Fig. 6. As shown in the figure, the overall roundness of the steel balls obtained by CWR is good and there are no obvious loose defects at the center of the balls by comparing the sectional images of the middle ball and side ball. This is because when the ideal ball diameter (i.e. the diameter of the die cavity) is 26 mm, using a billet with a diameter of 25 mm for hot CWR will cause the die cavity to be underfilled. And the extrusion pressure of the wedges on the middle ball and side balls is insufficient for the formation of loose defects in the steel balls.

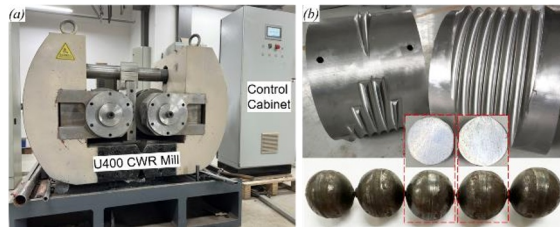


Fig. 6. **a** U400 CWR mill used in the experiments and **b** rollers and experimentally obtained bearing steel balls

As a comparative experiment, a GCr15 bearing steel rod with a diameter of 25.9 mm was used for steel balls forming. The experimental results shown in Fig. 7 showed that there was a significant central piercing in the middle ball and no loose defects on side ball. This is due to the fact that as the diameter of the billet increases, the die cavity becomes overfilled and the incompressible metal can only escape in the circumferential direction under the radial and axial compression of the wedges, causing the tensile stress at the center to exceed the limit, resulting in piercing defect.

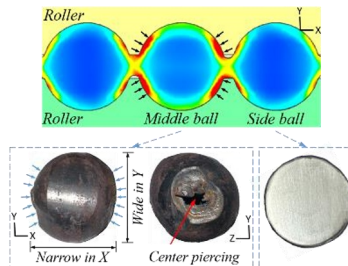


Fig. 7. Comparison experiment results of steel balls and numerical simulation diagram

3.3 Process improvement

Based on the above analysis, it can be concluded that the existing CWR bearing steel balls process has the problem of uneven strain distribution between the middle ball and side balls, which can lead to poor consistency in balls quality. Therefore, this section proposes the use of even numbered ball rolling (ENBR), which starts from the connector between steel balls and spreads sequentially to both sides to obtain even numbered steel balls shown in Fig. 8a. The same numerical simulation of improved method were conducted for analysis, as shown in Fig. 8b. It can be concluded that the steel balls formed by the improved method have a more uniform distribution of effective strain, which could avoid the defect of inconsistent strain distribution between the middle ball and side balls of the original method.

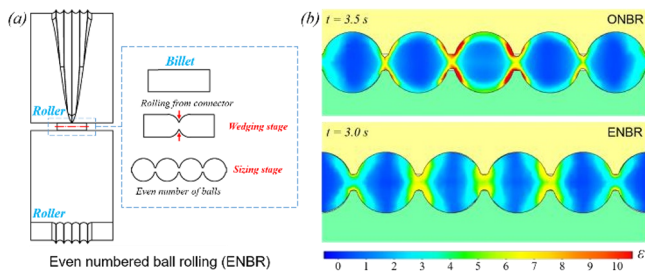


Fig. 8. **a** principle of process optimization and **b** comparison of effective strain of steel balls during forming process

4 Conclusions

- (1) The existing CWR bearing steel balls process has uneven distribution of effective strain between the middle ball and side balls, and the effective strain of the middle ball is significantly larger due to being squeezed by both wedges at the same time.
- (2) The three principal stresses at the center of the steel balls are all tensile stresses, with the effective stress at the middle ball being the highest.
- (3) When the die cavity is underfilled with billet, the steel balls have no central defects. When the die cavity is overfilled with billet, the steel balls have a high risk of central looseness. The risk of middle ball is significantly greater than that of side balls.
- (4) The method of ENBR can effectively address the problem of uneven distribution of effective strain in existing CWR steel balls and reduce the risk of central defects.

This work is supported by the National Natural Science Foundation of China (Grant No. 52275307), and Beijing Key laboratory of Metal Lightweight Forming and Manufacturing, China.

References

1. D. Qian, C. Ma, F. Wang, *Metals*, **11**, 456 (2021).
2. Y. Huo, T. He, B. Wang, Z. Zheng, Y. Xue, *Metall. Mater. Trans. A.*, **51**, 1254-1263 (2020).
3. Z. Pater, J. Tomczak, J. Bartnicki, M. Lovell, P. Menezes, *Int. J. Mach. Tool. Manu.*, **67**, 1-7 (2013).
4. T. Bulzak, K. Majerski, J. Tomczak, Z. Pater, Ł. Wójcik, *CIRP J. Manuf. Sci. Tec.*, **38**, 288-298 (2022).
5. Q. Cao, L. Hua, D. Qian, *J. Cent. South Univ.*, **22**, 1175-1183 (2015).
6. Z. Pater, J. Tomczak, T. Bulzak, Z. Cyganek, S. Andrietti, M. Barbelet, *Int. J. Adv. Manuf. Tech.*, **97**, 893-901 (2018).
7. J. Shen, B. Wang, C. Yang, J. Zhou, X. Cao, *J. Mater. Process. Tech.*, **294**, 117140 (2021).
8. J. Wang, B. Wang, Z. Fu, Z. Lai, *J. Mater. Process. Tech.*, **318**, 118036 (2023).